Journal of Computing and Electronic Information Management
ISSN: 2413-1660 | Vol. 20, No. 1, 2026

Structural Optimization of Shell-and-Tube Heat Exchanger Shell Side Based on Numerical Simulation and Response Surface Methodology

Zhizhong Lv [1], Hao Wen [1] *, Jiaqi Lv [2], Jiawei Liu [1], Linpeng Li [1]

[1] School of Mechatronic Engineering, Southwest Petroleum University, Chengdu, 610500, China
[2] Agricultural Economic Management station of Dachuan District, Dazhou 635700, China

[*] **Corresponding author**

Abstract: To enhance the shell-side heat transfer performance of shell-and-tube heat exchangers while balancing flow resistance, this study investigates a small-scale shell-and-tube heat exchanger. Using numerical simulation, it systematically analyzes the effects of structural parameters—including baffle spacing, baffle notch width, and tube-to-tube spacing—on shell-side flow and heat transfer characteristics. A three-dimensional numerical computational model based on the Realizable k-ε turbulence model was established and validated against experimental data. The simulation error for air outlet temperature was controlled within 6.5%, demonstrating good model reliability. Results indicate that increasing the number of baffles from 3 to 7 raised the average shell-side heat transfer coefficient by 23.63%, but significantly increased pressure drop. increasing the baffle notch width from 0.2D to 0.5D reduced the heat transfer coefficient by an average of 9.6%; increasing the tube spacing from 26 mm to 42 mm decreased the heat transfer coefficient by an average of 11.61%. Multi-parameter interaction analysis based on the response surface method indicates that the arrangement spacing and notch width of baffles exert the most significant influence on both the heat transfer coefficient and pressure drop.

Keywords: Shell and tube heat exchanger; Response surface optimization; Simulation analysis.

1. Introduction

In Chinas industrial production, energy utilization efficiency remains low at an average of less than 35% due to outdated equipment and technological backwardness, significantly below the 51%+ level achieved in Western countries [1]. In recent years, China has placed particular emphasis on advancing energy utilization [2]. Currently, heat exchangers come in diverse types, which can be categorized by structure and principle into shell-and-tube, plate, air-cooled, and spiral plate types [3]. Although shell-and-tube heat exchangers exhibit slightly weaker performance, their simple structure, low cost, and ease of maintenance make them highly valuable for engineering applications [4][5]. Research by Zhao Na and Wang Qiuwang indicates that spiral baffle heat exchangers offer lower pressure drop and higher overall performance compared to curved baffle heat exchangers under identical operating conditions. While increasing the spiral angle reduces heat transfer efficiency, it results in a more significant decrease in resistance [6][7].

Enhancing heat transfer in both the tube side and shell side is a key focus in shell-and-tube heat exchanger research. Shell-side heat transfer performance is typically analyzed through experimental studies and numerical simulations. Experimental results are relatively reliable but suffer from high costs and lengthy cycles, making their direct application in heat transfer enhancement studies prone to resource wastage. In contrast, numerical simulation methods have matured significantly in recent years, offering advantages such as short cycles, low costs, and strong parameter controllability, and have been widely adopted in heat exchanger research. This study focuses on shell-and-tube heat exchangers, establishing sound physical and mathematical models while defining fluid property parameters. A performance-based evaluation system is constructed to conduct numerical simulations of shell-side flow and heat transfer characteristics. Concurrently, standardized experimental protocols based on prototype equipment are developed to obtain test data under identical operating conditions, enabling quantitative validation of simulation results. This lays the foundation for subsequent single-objective and multi-objective optimization studies.

2. Numerical simulation

2.1. Numerical Methods/Mathematical Models

During simulation calculations, the flow of fluid in the shell side and energy exchange must obey the three fundamental conservation equations [8]. These equations provide the basic physical framework for fluid calculations, enabling the prediction and analysis of fluid flow characteristics through numerical simulation. The mass conservation equation can be expressed as:

$$\frac{\partial \rho}{\partial \mathrm{t}}+\frac{\partial(\rho u)}{\partial \mathrm{x}}+\frac{\partial(\rho v)}{\partial \mathrm{y}}+\frac{\partial(\rho w)}{\partial \mathrm{z}}=0$$

In the equation, ρ denotes the fluid density in kg/m³; t denotes time in seconds; u, v, and w denote the velocity vectors in the x, y, and z directions, respectively. The momentum conservation equation can be expressed as:

$$\frac{\partial(\rho u)}{\partial t}+\nabla(\rho u \bar{u})=\nabla(\delta gradu)-\frac{\partial p}{\partial x}+S_u$$

$$\frac{\partial(\rho v)}{\partial t}+\nabla(\rho v \bar{u})=\nabla(\delta gradu)-\frac{\partial p}{\partial y}+S_{\mathrm{v}}$$

$$\frac{\partial(\rho \mathrm{w})}{\partial t}+\nabla(\rho w \bar{u})=\nabla(\delta gradu)-\frac{\partial p}{\partial x}+S_w$$

In the equation, δ denotes dynamic viscosity, N•s/m²; u represents the velocity vector; P indicates pressure on a fluid element, S_u; S_v, S_w denote the generalized source terms of the momentum conservation equation. The energy conservation equation can be expressed as:

$$\frac{\partial(\rho T)}{\partial t}+\frac{\partial(\rho uT)}{\partial x}+\frac{\partial(\rho vT)}{\partial y}+\frac{\partial(\rho wT)}{\partial z}=$$

$$\frac{\partial}{\partial x}(\frac{\lambda}{C_p}\frac{\partial T}{\partial x})+\frac{\partial}{\partial y}(\frac{\lambda}{C_p}\frac{T}{\partial y})+\frac{\partial}{\partial}(\frac{\lambda}{C_p}\frac{\partial T}{\partial z})+S_T$$

In computational fluid dynamics, turbulence models play a crucial role, primarily used to simulate and predict turbulent characteristics during fluid flow. This paper selects the Realizable k-ε model for simulation and computational solutions. The transport equations for the Realizable k-ε turbulence model are as follows:

$$\frac{\partial}{\partial \mathrm{t}}(\rho k)+\frac{\partial}{\partial x_j}(\rho k u_j)=\frac{\partial}{\partial x_j}\left[\left(\mu+\frac{\mu_{\mathrm{t}}}{\sigma_k}\right)\frac{\partial k}{\partial x_j}\right]+G_k+G_b-\rho\varepsilon-Y_{\mathrm{M}}+S_k$$

$$\frac{\partial}{\partial \mathrm{t}}(\rho\varepsilon)+\frac{\partial}{\partial x_j}(\rho\varepsilon u_j)=$$

$$\frac{\partial}{\partial x_j}\left[\left(\mu+\frac{\mu_{\mathrm{t}}}{\sigma_\varepsilon}\right)\frac{\partial \varepsilon}{\partial x_j}\right]+\rho C_1 S\varepsilon-\rho C_2\frac{\varepsilon^2}{k+\sqrt{v\varepsilon}}+C_{1\varepsilon}\frac{\varepsilon}{k}C_{3\varepsilon}G_b+S_\varepsilon$$

In the equation, k denotes turbulent kinetic energy; ε represents the turbulent dissipation rate; σ_k and σ_ε denote the Prandtl numbers corresponding to turbulent kinetic energy k and dissipation ε, respectively; G_k and G_ε represent the production terms for turbulent kinetic energy k and dissipation rate ε induced by the mean velocity gradient, respectively; G_b denotes the production term for turbulent kinetic energy k induced by buoyancy forces; S denotes the modulus of the mean strain rate tensor; S_k and S_ε denote user-defined source terms; Y_M represents the contribution of pulsating expansion to the total dissipation rate in compressible turbulence; the constants in the equation are $C_{1\varepsilon}$=1.44, C_2=1.9, σ_k=1.0, and σ_ε=1.2.

2.2. Physical Model

The accuracy of the final results from numerical simulation calculations is highly dependent on the reliability of the physical model. Prior to Fluent computations, model simplification is a crucial step primarily aimed at reducing computational complexity, enhancing computational stability, and conserving time and resources. Based on the actual parameters of the heat exchanger, a three-dimensional model of the heat exchanger was constructed in 3D modeling software, as shown in Figure 1.

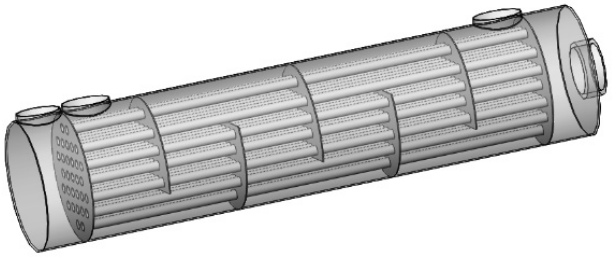

Figure 1. Three-dimensional model of the heat exchanger

The main geometric dimensions of the heat exchanger are shown in Table 1.

Table 1. Key Structural Parameters of Heat Exchangers

Name	Dimension Parameters
Housing Length/mm	1300
Housing Wall Thickness/mm	5
Baffle Plate Thickness/mm	2
Baffle Plate Spacing/mm	165
Heat Exchange Tube Outer Diameter/mm	20
Heat Exchange Tube Length/mm	1000
Heat Exchange Tube Wall Thickness/mm	1
Number of Heat Exchange Tubes/pcs	31
Heat Exchange Tube Spacing/mm	34
Heat Exchange Tube Material	Q235 Steel

2.3. Boundary Conditions and Network Partitioning

In Fluent, boundary conditions are a crucial component for defining fluid flow and heat transfer problems. They describe the behavior of the fluid at the boundaries of the computational domain, ensuring the accuracy and physical validity of the simulation. In the numerical model of the heat exchanger, the inlet boundary employs a mass flow condition to set the flow flux parameters, while the outlet boundary is defined based on pressure conditions. This compact biomass heat exchanger generates heat at a rate of Qout = 10 × 10⁴ kJ/h, with a thermal efficiency of approximately 70%.

The inlet temperature of the cold air is set at 30°C. According to the heat exchanger design requirements, the cold air must be discharged at 120°C, resulting in a temperature difference of Δ_{t2}= 90°C. For air with a specific heat capacity C_ρ = 1.201 J/kg•K, the mass flow rate at the air inlet is m = 0.18 kg/s. The basic boundary conditions for the heat exchanger are set as shown in Figure 2.

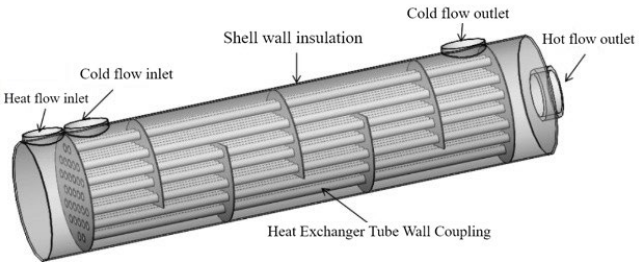

Figure 2. Basic Boundary Condition Settings

Grid independence refers to the property where simulation results remain consistent regardless of the number of grid cells used in numerical computations, thereby minimizing simulation errors. By varying the grid count according to the aforementioned partitioning method, six grid configurations were created with respective cell counts of 1.25 million, 1.9 million, 2.53 million, 3.47 million, 4.63 million, and 5.41 million. With identical boundary parameters applied, the computational results are presented in Figure 3. Beyond 3.47 million grid cells, the trends in outlet temperature and pressure difference become relatively stable. Comparing the calculated air outlet temperature and shell-side pressure difference across different grid sizes, the relative errors for the

3.47 million and 4.63 million grid cell configurations were 1.31% and 0.59%, respectively. Therefore, to conserve computational resources while ensuring accuracy, the 3.47 million-cell grid model is adopted for subsequent simulation calculations in this study.

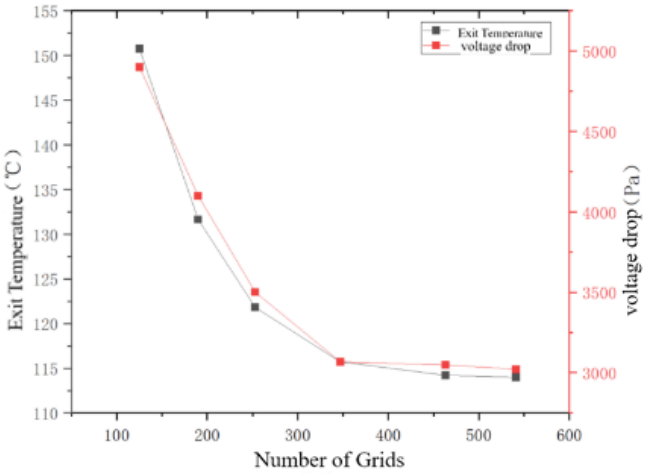

Figure 3. Verification Results of Mesh Independence for Different Mesh Models

2.4. Validation and Evaluation Criteria

To ensure the accuracy of the numerical simulation study in this paper, tests were conducted on the heat exchanger prototype. Under steady-state operating conditions, temperature and air velocity variations at the outlet were recorded. During operation, outlet temperature was measured and logged every minute, while outlet velocity was measured and logged every 10 seconds. The compiled data yielded the temperature and flow variation plots shown in Figure 4. The plots reveal that the heat exchanger outlet temperature stabilized after approximately 8 minutes, while the mass flow rate at the outlet rapidly reached equilibrium within the first 50 seconds of operation. Test conditions under this operating state were: air inlet mass flow rate of 0.18 kg/s, ambient temperature of 27°C, and flue gas mass flow rate of 0.04 kg/s. Simulation calculations under these conditions yielded an outlet temperature of 115.68°C. Compared to experimental data, this represents a temperature difference of approximately 8.03°C, with an error margin of about 6.49%. The comparison indicates that the simulation error falls within acceptable limits, confirming the applicability of this simulation model for the present study.

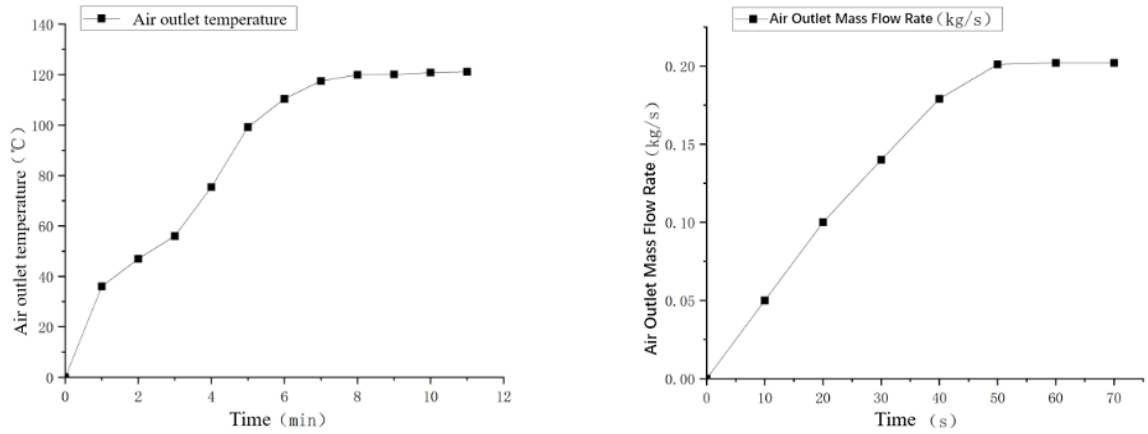

Figure 4. Temperature and Mass Flow Rate at the Air Outlet as a Function of Time

The single-performance evaluation method assesses heat exchanger performance using a single metric, offering a straightforward approach that facilitates rapid analysis and comparison [9][10]. This paper focuses on optimizing the shell-side structure of heat exchangers to achieve simultaneous enhancement of heat transfer efficiency and flow characteristics, thereby maximizing overall heat transfer performance. Consequently, performance evaluation metrics from current engineering research are adopted to analyze changes in heat exchanger performance: the heat transfer coefficient h is used to evaluate heat transfer performance, while the pressure drop ΔP serves as the resistance performance evaluation coefficient.

3. The Effect of Different Parameters on Heat Exchanger Performance

Figure 5 indicates that heat transfer dead zones in the shell side primarily occur near the backflow surface of the baffles. As the baffle spacing increases from 125 mm to 250 mm (reducing the number of baffles from 7 to 3), both the shell-side flow velocity and turbulence intensity decrease. This expansion of heat transfer dead zones results in an average reduction of 23.63% in the shell-side heat transfer coefficient.

When the baffle notch width increased from 0.2D to 0.5D, fluid bypassing intensified and the scouring effect on the heat transfer tubes weakened, resulting in an average decrease of 9.6% in the shell-side heat transfer coefficient. Furthermore, reducing the tube spacing from 42 mm to 26 mm increases the flow velocity and turbulence intensity in the tube bundle region, resulting in an average increase of 11.61% in the shell-side heat transfer coefficient. The results indicate that appropriately reducing the baffle spacing and tube spacing while controlling the baffle notch width helps mitigate heat transfer dead zones and enhance shell-side heat transfer performance.

Figure 6 comprehensively illustrates the influence of structural parameters and mass flow rate on the shell-side heat transfer coefficient. As the number of baffles increased from 3 to 7, the shell-side heat transfer coefficient rose overall, achieving an average improvement of 23.63% under identical mass flow conditions. However, the rate of increase markedly diminished when the number of baffles exceeded 6, indicating that the enhancement effect approached saturation. When the

baffle notch width increased from 0.2D to 0.5D, the shell-side heat transfer coefficient decreased overall, with an average reduction of 9.6%. When the tube spacing increased from 26 mm to 42 mm, the heat transfer coefficient decreased by an average of 11.61%. Furthermore, under fixed structural parameters, increasing the mass flow rate from 0.1 kg/s to 0.3 kg/s enhances the shell-side heat transfer coefficient. However, the rate of increase diminishes progressively with higher flow rates, indicating an upper limit to the flow rates contribution to heat transfer enhancement.

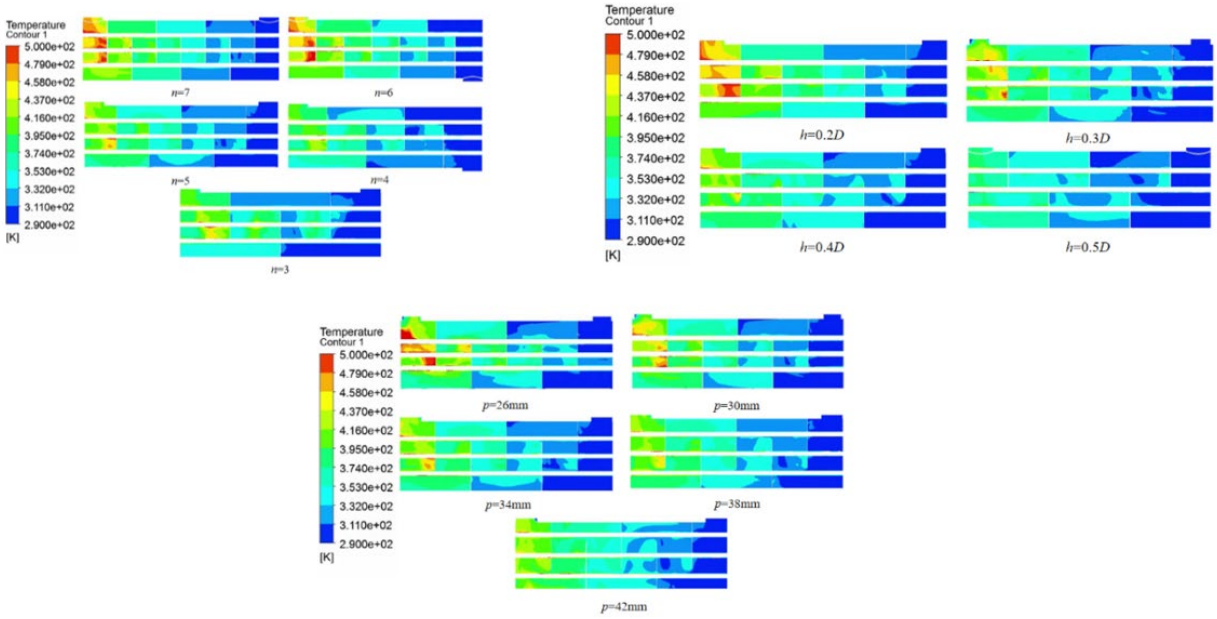

Figure 5. Shell-side Fluid Temperature Diagram for Various Parameters

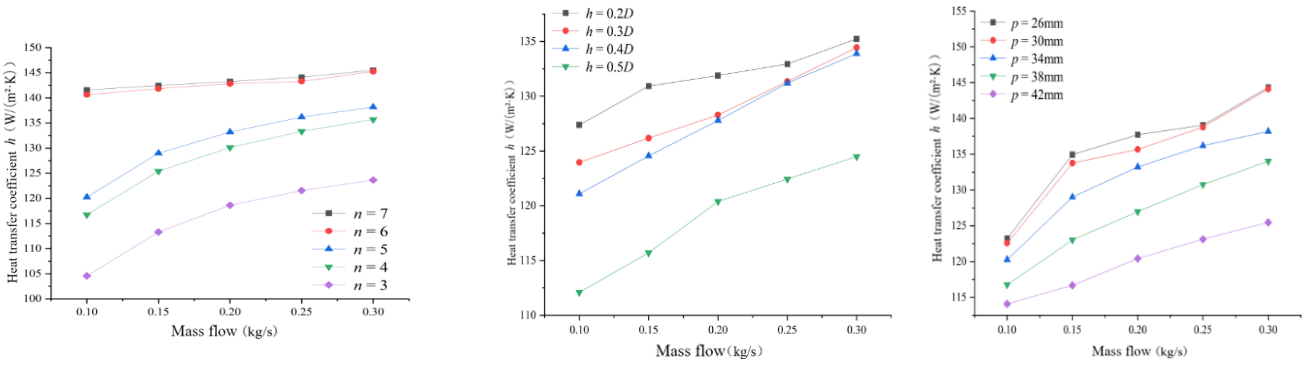

Figure 6. Heat Transfer Coefficient Variation Diagram Under Different Parameters

4. Optimization Analysis of Heat Exchangers Based on Response Surface Methodology

The heat transfer coefficient serves as the response indicator, yielding a response surface depicting the interaction between baffle spacing, baffle notch width, overall heat transfer tube spacing, and flow parameters, as shown in Figure 7. The shape of the response surface and the density of contour lines reflect the influence of each parameter on the heat transfer coefficient. The effects of baffle spacing and baffle gap width on the heat transfer coefficient are significantly greater than that of the overall heat transfer tube spacing. Among these, the interaction between baffle gap width and overall heat transfer tube spacing is the most pronounced. When both baffle spacing and gap width decrease, the overall heat transfer coefficient increases. However, excessively narrow gaps cause the coefficient to decline. Increasing either air or flue gas mass flow rate enhances the heat transfer coefficient, though their combined effect is relatively weak.

Using pressure drop as the response metric, an interaction response surface was constructed for the combined effects of baffle spacing, baffle notch width, overall heat transfer tube spacing, and flow parameters, as shown in Figure 8. The combined influence of baffle spacing and baffle notch width on pressure drop was found to be the most significant. As the baffle spacing decreased from 250 mm to 125 mm and the baffle gap width decreased from 135 mm to 54 mm, the shell-side pressure drop increased significantly. When both the baffle spacing and the overall heat transfer tube spacing decreased simultaneously, the pressure drop also showed an upward trend. Among the flow parameter interactions, the air mass flow rate had a significantly greater impact on pressure drop than the flue gas mass flow rate.

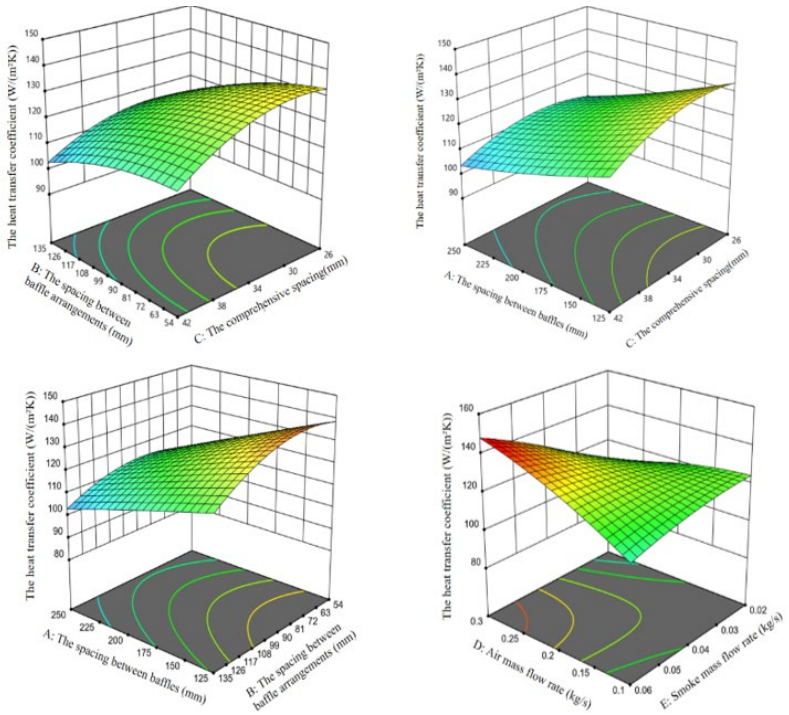

Figure 7. Three-dimensional response surface plot of heat transfer coefficient h

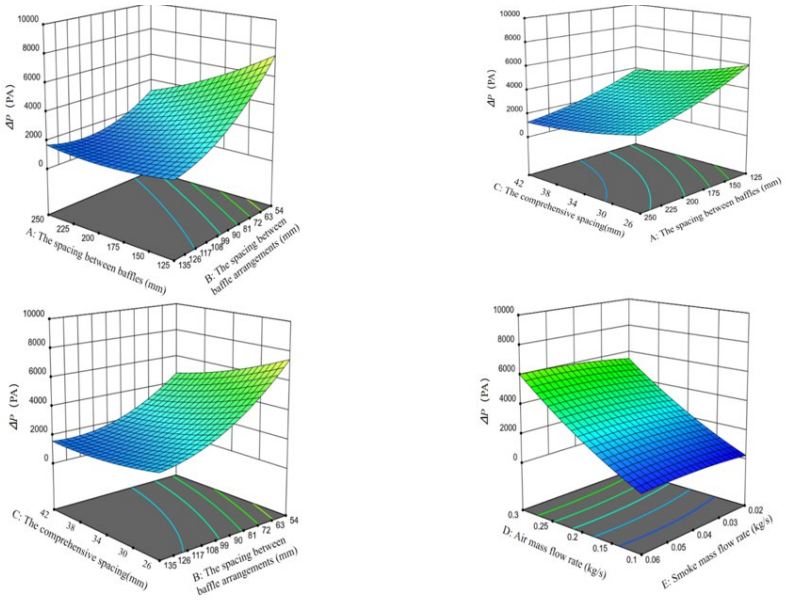

Figure 8. Three-dimensional response surface plot of pressure drop ΔP

5. Conclusion

This study investigates shell-and-tube heat exchangers using a combined approach of numerical simulation and experimental validation. It systematically analyzes the influence of shell-side structural parameters and flow parameters on heat transfer and flow characteristics, and conducts performance optimization based on the response surface method. Results demonstrate good agreement between numerical simulations and experimental data, with air outlet temperature errors controlled within 6.5%, validating the reliability of the established physical model, mathematical model, and boundary conditions. The spacing of baffles significantly impacts shell-side heat transfer and flow characteristics. Reducing baffle spacing enhances fluid turbulence and mixing, decreases dead zones, and improves the heat transfer coefficient. However, this leads to a marked increase in shell-side pressure drop. Furthermore, the heat transfer enhancement effect tends toward saturation when the number of baffles exceeds a certain threshold. The width of baffle notches plays a decisive role in shell-side bypass flow. Increasing notch width weakens tube bundle scouring and reduces heat transfer performance. Conversely, excessively narrow notches, while beneficial for heat transfer enhancement, significantly increase pressure drop. Therefore, their value requires comprehensive trade-off consideration. Reducing tube spacing increases flow velocity and turbulence intensity within the tube bundle, enhancing shell-side heat transfer. However, excessively narrow spacing also increases flow resistance. Response surface analysis results further indicate that the influence of baffle spacing and baffle gap width on heat transfer coefficient and pressure drop is significantly greater than that of overall tube spacing. Among flow parameters, air mass flow rate has a markedly greater impact on pressure drop than flue gas mass flow rate. The established response surface model provides effective

reference for multi-objective optimization design of shell-side structural parameters in shell-and-tube heat exchangers.

References

[1] Sun Yue. Numerical Study and Optimal Design of Shell-Side Heat Transfer and Flow Performance in Shell-and-Tube Heat Exchangers [D]. Huazhong University of Science and Technology, 2021. DOI: 10.27157/d.cnki.ghzku.2021.001882.

[2] National Development and Reform Commission. Modern Energy System Plan for the 14th Five-Year Plan Period [R], 2022.

[3] Zhu Dongsheng, Qian Songwen, Ma Xiaoming, et al. Heat Exchanger Technology and Advances [M]. Beijing: China Petrochemical Press, 2008.

[4] Qian, Songwen. Heat Exchanger Design Manual. Beijing: Chemical Industry Press, 2002.

[5] Dong Qiwu, Liu Minshan. Downflow Shell-and-Tube Heat Exchanger [M]. Beijing: Chemical Industry Press, 2007.

[6] Zhao Na, Song Tianmin, Zhang Guofu, et al. Study on Heat Transfer Enhancement in the Shell Side of Spiral Baffle Tube-Shell Heat Exchangers [J]. Refining Technology and Engineering, 2007, (01): 38-41.

[7] Wang Qiuwang. Research Progress on Heat Transfer Enhancement in the Shell Side of Spiral Baffle Tube Shell-and-Tube Heat Exchangers [J]. Journal of Xi'an Jiaotong University, 2004, (09): 881-886.

[8] Tao, Wenquan. Numerical Heat Transfer [M]. Xi'an: Xi'an Jiaotong University Press, 2001.

[9] Yu, Jianzhu. Heat Exchanger Principles and Design. Beijing: Beihang University Press, 2006.

[10] Liu Yan. Experimental Study and Performance Evaluation of Plate Heat Exchangers [D]. Changchun: Jilin University, 2001.